Modeling and Control of Solar-Grade Silicon Production in a Fluidized Bed Reactor

Juan Du, Soham Dutta, and Birger Erik Ydstie
Dept. of Chemical Engineering, Carnegie Mellon University, Pittsburgh, PA 15213

DOI 10.1002/aic.14378
Published online March 5, 2014 in Wiley Online Library (wileyonlinelibrary.com)

A multiscale model predicts silicon production yield and powder loss in a fluidized bed reactor for solar silicon production. The reaction module calculates the silicon vapor deposition and powder scavenging rates. A computational fluid dynamics model predicts temperature and bed density. A population balance model calculates the particle-mass distribution functions on silicon yield. The model results are validated against industrial data. Furthermore, we conduct a sensitivity analysis to investigate the effect of gas flow rate and inlet silane concentration. Finally, a control strategy is proposed to maintain the process at the desired operating point. © 2014 American Institute of Chemical Engineers *AIChE J*, 60: 1740–1751, 2014

Keywords: solar-grade silicon production, multiscale modeling, sensitivity analysis, inventory control, fluidized bed reactor

Introduction

Solar photovoltaic industry has experienced a remarkable growth over the last decade. Even during a time of economic crisis, global cumulative photovoltaic capacity still increased rapidly. The world's cumulative photovoltaic capacity surpassed 100-GW installed electrical power last year. Each year, these photovoltaic installations save more than 53 million tons of carbon dioxide emissions.[1] However, high prices of photovoltaic cells have bottlenecked them to be cost competitive in the worldwide electricity market. Among this total manufacturing cost, solar-grade silicon production takes up to 20% and therefore there exists a significant incentive to reduce feedstock production cost.[2] As a result, photovoltaic industry has been searching for new methods of silicon production and production in fluidized bed reactors (FBR) is one feasible approach. Due to the complex characteristics of FBR, modeling and control of such processes are never an easy task. Extensive research has been carried out to investigate the silicon production in FBR. However, most of them focused on certain specific aspects of laboratory experiments and computational fluid dynamics modeling. A comprehensive model to calculate and predict the amount of silicon powder lost and the resulting final product size is still missing. Furthermore, this model serves as a basis for model-based control design. The objective of this work is to develop a multiscale model for solar-grade silicon production in a FBR to predict silicon yield and then to control the average size of silicon particle product by designing an inventory control system.

The earliest studies of silicon production from high-purity silane feedstock using a FBR were conducted by Union Carbide Corporation and Jet Propulsion Laboratory.[3] The research program was funded partially by Department of Energy in an attempt to jump start the photovoltaic industry in the United States in the aftermath of the energy crisis in the early 1970s. The research program included both theoretical and experimental components. Lai et al.[4] developed a model of the system to investigate the reaction mechanism for thermal pyrolysis of silane in a FBR. The model predictions were validated against experiments conducted at Jet Propulsion Laboratory. This modeling approach was inspired by two-phase models that divide the FBR into an emulsion phase and a bubble phase. Such models were classified into four categories: the Patridge and Rowe model; the Kunii–Levenspiel model; the modified Kunii–Levenspiel model; and the Kato–Wen model.[5,6] All models assume that mass and heat are exchanged between the bubble and the emulsion phase. Caussat et al.[7] tested these models in small-scale experiments. They found out the Kato–Wen model gave the best agreement with experimental data. They claimed that powders in the process were formed by wall deposition of the various polymeric Si species rather than by homogeneous decomposition of silane, which was in contradiction to Lai's findings.[8] Pina et al.[9] developed a dynamic model for a spouted-bed reactor similar to that developed by Lai.[8] They modeled the process with a jet emulsion and a bubble emulsion region. One major difference is that Pina et al. used the method of characteristics to discretize the population balance and to predict particle-size distribution, whereas Lai used the method of moments to capture the dynamics of powders. Huang et al.[10] modified the two-phase model by treating the emulsion phase as a number of interconnected well-mixed tanks rather than one single well-mixed tank. The modified model provided reasonable agreement with experimental data obtained from an industrial pilot plant. Guenther et al.[11] developed the Euler–Euler continuum approach for simulating FBR using the Multiphase Flow with Interphase eXchanges (MFIX) System developed at National Energy

Correspondence concerning this article should be addressed to B.E. Ydstie at ydstie@cmu.edu.

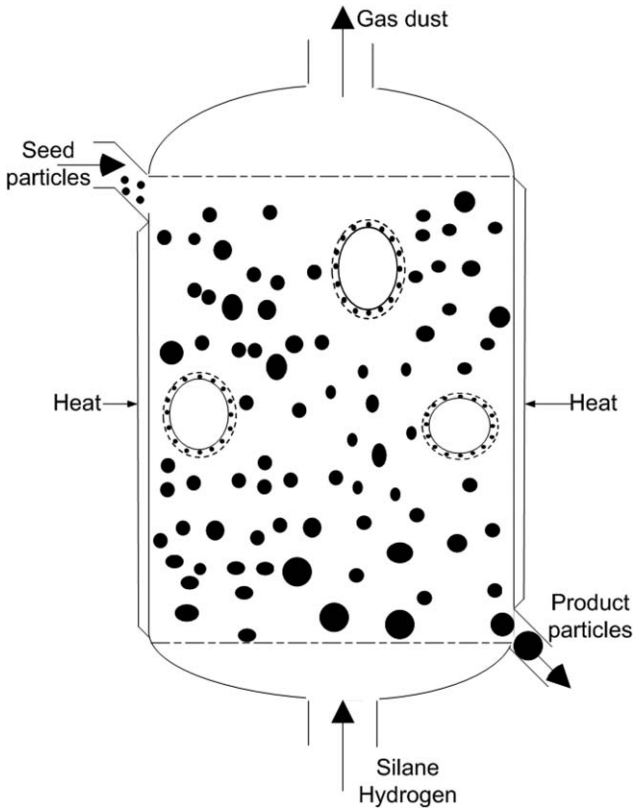

Figure 1. A schematic diagram of FBR.

Technology Laboratory. Caussat and coworkers[12] conducted transient simulations for silicon fluidized bed chemical vapor deposition from silane on coarse powders. The numerical model developed by Cadoret et al.[13] predicted the temporal and spatial evolutions of local void fractions, gas and particle velocities, and silicon deposition rate. Experimental studies[14] showed that silane conversion was quite complete and powder formation limited when the inlet concentration of silane was less than 20%.

White et al.[15] developed a modeling technique to describe the particle phase by combining the mass and number balances. The model uses ordinary differential and algebraic equations to track particle movement through discrete size intervals to simulate changes in the size distribution. Furthermore, they showed that the conversion of silane to silicon is effectively complete over a length scale of centimeters at the entrance of the reactor, whereas the gas flow rate changes over the entire reactor height (in the order of meters). This changes the bed density which influences the silicon yield. The particle-size distribution reaches steady state at a time scale in the order of days.[15] Thus, time scales range from seconds to days, whereas length scales varies from μm to meters. Sukumar et al.[16] proposed to use multiscale modeling technique for polysilicon production in the FBR. Du and Ydstie[19] investigated the stability property and control strategy for solar grade silicon production process in this FBR.

The aim of this work is to develop a model to predict the silicon yield as a function of operating conditions. Such a model can then be used for control and optimization studies. The proposed model is validated using the experimental data from a pilot-scale reactor. The sensitivity analysis shows that the increase of flow rate or inlet silane concentration results in faster particle growth rate. However, if we increase the molar fraction of silane in the feed gas, then power loss increases while deposition rate goes up. Therefore, maximizing silicon deposition rate and minimizing powders loss are two conflicting objectives when we adjust the molar fraction of silane. A trade-off has to be made to meet these competing requirements. An inventory control system is designed to maintain the fluidized bed at the desired operating condition.

Multiscale Modeling Approach for FBR

The schematic diagram of the FBR for polysilicon production is illustrated in Figure 1. The bed is preloaded with silicon seed particles to initiate silicon deposition. A preheated gas mixture of silane and hydrogen enters at the bottom of the bed to fluidize silicon particles. As the bed is heated to reaction temperature, silane thermally decomposes to solid silicon and hydrogen by the pyrolysis which is governed by the overall reaction

$$SiH_4 \rightarrow Si + 2H_2 \quad (1)$$

The reaction is fast and goes to completion if the reaction temperature is above 650°C. In addition to chemical reaction, there are many other physical transformations that need to be accounted for. Homogeneous polymerization reactions take place as silane reacts to form amorphous powders in the vapor phase. Silicon powder is scavenged by particles in the reactor and converted to silicon which contributes to particle growth. The remainder is exhausted with the hydrogen gas. The silicon yield in the form of Silicon deposited on seed particles is low if a large amount of powder is lost through gas exhaustion and hence the process economics suffer.

One important objective of this work is to develop a model to predict powder loss and operational strategies that can be used to minimize powder loss. Another goal is to stabilize and control the particle growth process such that silicon granules with predictable and uniform size distribution are produced. As different temporal and spatial scales are present in the FBR process, we decompose the model into three distinct modules and develop information communication among the modules as shown in Figure 2.

The fluid dynamics module describes the hydrodynamics by predicting pressure drop, bed expansion, and temperature profile. Physical properties used in the model were taken from several references [17] [18]. This module also accounts for thermal decomposition of silane and powder formation by polymerization which occur in the vessel scale. The particles are well-mixed and their average size changes slowly. We therefore assume the fluidization conditions are unchanged as seen from the reaction and hydrodynamics process viewpoint. The fluid dynamics module is implemented using COMSOL.

A reaction module accounts for reaction kinetics and calculates silicon deposition and particle growth rates based on the information provided by the fluid dynamics module.

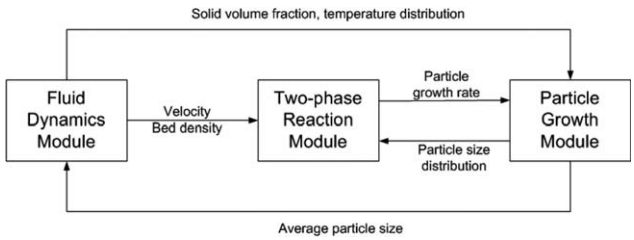

Figure 2. Multiscale model structure.

These reactions take place in fractions of a second, whereas temperature changes that impact reaction and deposition rates have time-scale in the order of minutes.

Particle growth rate serves as the key parameter for the discrete population balance to capture the evolution of particle-size distribution. The particle-size distribution reaches steady state in the order of days as evidenced by simulation studies and experimental results. The bed temperature and solid volume fraction profiles along bed height are generated from a fluid dynamics module and imported into reaction module. Silicon vapor deposition rate and powder scavenging rate are calculated based on the updated operating condition. These key parameters are required in the population balance module to obtain particle growth rate. Once the mass-transfer rate is determined, particle-size distribution is calculated by solving mass balance equations. The particle-size distribution has a major impact on the fluidization behavior of the bed and the particle-size distribution is thus used in fluid dynamics module to refresh the fluidization condition periodically.

The two-phase reaction module

The reaction module is adapted from the two-phase fluidized bed model developed by Lai.[8] The bubble and emulsion phases describe the silicon production from silane pyrolysis. The reactant gas flows through bubbles and the emulsion phase. Small bubbles form near the distributors at the bottom of the reactor and rise while growing. Mass and heat transfer take place between two adjacent phases.

In the bubble phase, polysilicon is produced by homogeneous reaction. In the emulsion phase, the silane vapor either deposits on seed particles by chemical vapor deposition or it dimerises to form polysilicon in the vapor phase. Silicon vapor phases nucleate through molecular bombardment or conventional nucleation to form the nuclei with critical size which grow by coagulation to form a brown amorphous powder. These powders may leave the reactor, resulting in yield loss; they also can be scavenged by existing silicon particles in the bed. Experiments have shown that the powders do not agglomerate to form silicon particles. Thus, new seed particles need to be added at the same rate as particles are withdrawn.

Silane thermally decomposes through two independent pathways. One is the homogeneous decomposition into a gaseous precursor that is scavenged by silicon particles. The rate of homogeneous decomposition of silane is given by[20]

$$r_{\mathrm{HD}} = 2\times10^{13}\exp\left(-26000/T_e\right)c_S \tag{2}$$

Silicon nuclei are produced by homogeneous nucleation which is described by the theory developed by Volmer et al. The rate of homogeneous nucleation is given as[21]

$$r_{\mathrm{HN}} = N_{\mathrm{A}}\frac{\alpha_c}{\rho}\left(\frac{2\bar{\sigma}m}{\pi}\right)^{1/2}\exp\left(-\frac{4\pi\bar{r}^2\sigma N_{\mathrm{A}}}{3\mathrm{RT}_e}\right)c_{\mathrm{Si}}^{*2} \tag{3}$$

where N_{A} is Avogadro's number and α_c is condensation coefficient. $\bar{\sigma}$ is the specific surface energy which is calculated by

$$\bar{\sigma} = \bar{\sigma}_1\left(\frac{7500-T_e}{7500-T_1}\right)^{1.2} \tag{4}$$

$\bar{r}$ denotes the critical radius as

$$\bar{r} = \frac{2\bar{\sigma}M_{\mathrm{Si}}}{\rho_p RT_e \ln P_{\mathrm{Si}}/P_{\mathrm{Si}}^0} \tag{5}$$

where P_{Si}^0 is silicon vapor pressure at equilibrium. It is calculated by the expression

$$\log\left(760P_{\mathrm{Si}}^0\right) = -13.639 - 34072/T_e + 15.758\log T_e - 0.016158\,T_e + 0.0000023\,T_e^2 \tag{6}$$

Homogeneous decomposition generates silicon vapor. The concentration of silicon vapor is suppressed by diffusion and condensation on large particles and by molecular bombardment of powders. The rate of molecular bombardment of silicon vapor to form powders is calculated as[22]

$$r_{\mathrm{DF}} = \left(\frac{\mathrm{RT}}{2\pi M_{\mathrm{Si}}}\right)^{0.5}\left(c_{\mathrm{Si}} - c_{\mathrm{Si}}^*\right) \tag{7}$$

The other pathway is the heterogeneous decomposition of silane on the existing silicon seed particles or on the created nuclei leading to a chemical vapor deposition. The rate of heterogeneous chemical vapor deposition of silane is described by[23]

$$r_{\mathrm{HT}} = \frac{5.14\times10^9}{6\epsilon_b/d_p}\exp\left(-19530/T_e\right)c_S \tag{8}$$

The rate of molecular diffusion of silicon vapor onto larger particle is given as[22]

$$r_{\mathrm{DL}} = 2D_{\mathrm{g}}\left(c_{\mathrm{Si}} - c_{\mathrm{Si}}^*\right)/d_{\mathrm{p}} \tag{9}$$

here D_g is the molecular gas diffusion coefficient and is calculated as

$$D_{\mathrm{g}} = k_B T_e/\left(3\pi\mu d_{p,f}\right) \tag{10}$$

The total deposition rate r_{dep} is the sum of the heterogeneous rate, the molecular diffusion rate of silicon vapor and the scavenging rate, that is

$$r_{\mathrm{dep}} = A_{\mathrm{TL}}\left(r_{\mathrm{HT}} + r_{\mathrm{DL}}\right)M_{\mathrm{Si}} + m_{\mathrm{sca}} \tag{11}$$

where the scavenging rate of powders by large particles m_{sca} as

$$m_{\mathrm{sca}} = VI\rho_{\mathrm{Si}}\,\alpha M_1 \tag{12}$$

where α is the scavenging coefficient. It is calculated as

$$\alpha = Eu_{mf}\frac{3(1-\epsilon_{mf})}{2d_{p,f}\epsilon_{mf}} \tag{13}$$

where ϵ_{mf} and u_{mf} are bed voidage and superficial gas velocity. These time varying parameters are obtained from the fluid dynamics module described below. E is the single large particle collection efficiency which is the sum of efficiency for impaction, interception, and diffusion. The diffusive mechanism dominates under the conditions prevailing in the FBR and we calculate E as follows

$$E = 2\left(3\frac{d_p^2 u_{mf}\pi\mu}{k_B T_e}\right)^{-\frac{2}{3}} \tag{14}$$

The two-phase model assumes that the emulsion phase is at the minimum fluidization velocity and that the rest of the gas flows as bubbles. The bubble phase is surrounded by small amounts of solid particles that are carried upwards by the bubble. The bubbles, formed at the distributor grow while they

pass through the reactor and this variation in size is captured in the model using correlations for the minimum, the maximum bubble size, and the bubble volume fraction. The mass-transfer coefficients K_{ce} and K_{bc} account for mass-transfer rate between two phases, whereas heat-exchange coefficients H_{ce} and H_{bc} for thermal energy transfer between two phases. The transfer coefficients from bubble to cloud and transfer coefficients from cloud to emulsion are calculated as

$$K_{bc}=4.5\frac{u_{mf}}{d_p}+5.85\frac{D^{1/2}g^{1/4}}{d_p^{5/4}} \tag{15}$$

$$K_{ce}=6.77\sqrt{\frac{D\epsilon_c u_b}{d_p^3}} \tag{16}$$

$$H_{bc}=4.5\frac{u_{mf}\rho C_p}{d_p}+5.8\frac{(k\rho C_p)^{1/2}g^{1/4}}{d_p^{5/4}} \tag{17}$$

$$H_{ce}=6.77\sqrt{\frac{k\rho C_p\epsilon_c u_b}{d_p^3}} \tag{18}$$

where D is the particle diffusion coefficient and is given by

$$D=\frac{kT}{3\pi\mu d_p} \tag{19}$$

The overall transfer coefficients K_{be} are given by

$$\frac{1}{K_{be}}=\frac{1}{K_{bc}}+\frac{1}{K_{ce}} \tag{20}$$

$$\frac{1}{H_{be}}=\frac{1}{H_{bc}}+\frac{1}{H_{ce}} \tag{21}$$

The reaction module provides the information needed to predict the powder loss from the bed. We are not interested in a precise description of the size distribution of powder particles to predict loss. Therefore, we solve the population balance approximately using the method of moments.

The interchange coefficient for the powder flow between the bubble and emulsion phases, K_{be}, is assumed to be constant. We consider that the powder behaves like gas in both phases. The powder loss is calculated using the following formula

$$\text{Powder loss}=1-\frac{\mathrm{r_{dep}}}{(q_f c_{s,f}-(A_t u G_e c_{S,e}+A_t\delta_b\mu_b c_{s,b}))M_{\mathrm{Si}}} \tag{22}$$

Mass and energy balances in bubble phase

The detailed model illustrations about mass and energy balances in two phased can be found in Ref. 24. Here we list the model equations as follows:

Mass balance for SiH_4

$$\frac{d(u_{Gb}c_{S,b})}{dz}=\delta_b(K_{\mathrm{be}})_{b,S}(c_{S,e}-c_{S,b})-\delta_b r_{\mathrm{HD},b}-\delta_b\frac{(4\pi)^{1/3}3^{2/3}}{\phi_S}M_{2/3,b}r_{\mathrm{HT},b}$$

Mass balance for H_2

$$\frac{d(u_{Gb}c_{H,b})}{dz}=\delta_b(K_{\mathrm{be}})_{b,H}(c_{H,e}-c_{H,b})+2\delta_b r_{\mathrm{HD},b}+2\delta_b\frac{(4\pi)^{1/3}3^{2/3}}{\phi_S}M_{2/3,b}r_{\mathrm{HT},b}$$

Mass balance for Si vapor,

$$\frac{d(u_{Gb}c_{\mathrm{Si},b})}{dz}=\delta_b(K_{\mathrm{be}})_{b,\mathrm{Si}}(c_{\mathrm{Si},e}-c_{\mathrm{Si},b})+\delta_b r_{\mathrm{HD},b}-\delta_b\frac{(4\pi)^{1/3}3^{2/3}}{\phi_S}M_{2/3,b}r_{\mathrm{DF},b}-\delta_b r_{\mathrm{HN},b}$$

The energy balance is

$$\bar{c}_{\mathrm{pb}}\frac{u_{Gb}}{T_b}\frac{\pi}{R_{\mathrm{g}}}\frac{dT_b}{dz}=\delta_b(H_{\mathrm{be}})_b(T_e-T_b)+(-\Delta H_r)\delta_b r_{\mathrm{HD},b}+(-\Delta H_r)\delta_b\frac{(4\pi)^{1/3}3^{2/3}}{\phi_s}M_{2/3,b}r_{\mathrm{HT},b}$$

The inlet conditions at the bottom of the bed $z=0$ are specified as

$$c_{S,b}=c_{S,f}/\frac{T_e(1-\delta_{b0})+T_f\delta_{b0}}{T_f}$$

$$c_{H,b}=c_{H,f}/\frac{T_e(1-\delta_{b0})+T_f\delta_{b0}}{T_f}$$

$$C_{\mathrm{Si},b}=0$$

$$T_b=T_f$$

where δ_{b0} is the initial bubble void fraction and it is found by solving the following two algebraic equations simultaneously

$$u_0=\frac{q_f}{A_t}\frac{T_e(1-\delta_{b0})+T_f\delta_{b0}}{T_f}$$

$$\delta_{b0}=\frac{u_0-u_{mf}}{u_0-2u_{mf}+0.711(gd_{b0})^{1/2}}$$

Mass and energy balances in emulsion phase

Mass balance for SiH_4

$$\frac{d(u_{Ge}c_{S,e})}{dz}=\delta_b(K_{\mathrm{be}})b,\ S(c_{S,b}-c_{S,e})-(1-\delta_b)\epsilon_{mf}r_{\mathrm{HD},e}-(1-\delta_b)\epsilon_{mf}\frac{(4\pi)^{1/3}3^{2/3}}{\phi_S}M_{2/3,e}r_{\mathrm{HT},e}-\frac{6(1-\epsilon_{mf})}{\phi_S d_p}(1-\delta_b)r_{\mathrm{HT},e}$$

Mass balance for H_2

$$\frac{d(u_{Ge}c_{H,e})}{dz}=\delta_b(K_{\mathrm{be}})b,\ H(c_{H,,b}-c_{H,e})+2(1-\delta_b)\epsilon_{mf}r_{\mathrm{HD},e}+2(1-\delta_b)\epsilon_{mf}\frac{(4\pi)^{1/3}3^{2/3}}{\phi_S}M_{2/3,e}r_{\mathrm{HT},e}+2\frac{6(1-\epsilon_{mf})}{\phi_S d_p}(1-\delta_b)r_{\mathrm{HT},e}$$

Mass balance for Si polymer chains in the vapor phase

$$\frac{d(u_{Ge}c_{\mathrm{Si},e})}{dz}=\delta_b(K_{\mathrm{be}})b,\ \mathrm{Si}\,(c_{\mathrm{Si},b}-c_{\mathrm{Si},e})+(1-\delta_b)\epsilon_{mf}r_{\mathrm{HD},e}-(1-\delta_b)\epsilon_{mf}\frac{(4\pi)^{1/3}3^{2/3}}{\phi_S}M_{2/3,e}r_{\mathrm{DF},e}-\frac{6(1-\epsilon_{mf})}{\phi_S d_p}(1-\delta_b)r_{\mathrm{HT},e}-(1-\delta_b)\epsilon_{mf}r_{\mathrm{HN},e}$$

The inlet conditions at the bottom of the bed $z=0$ are specified as

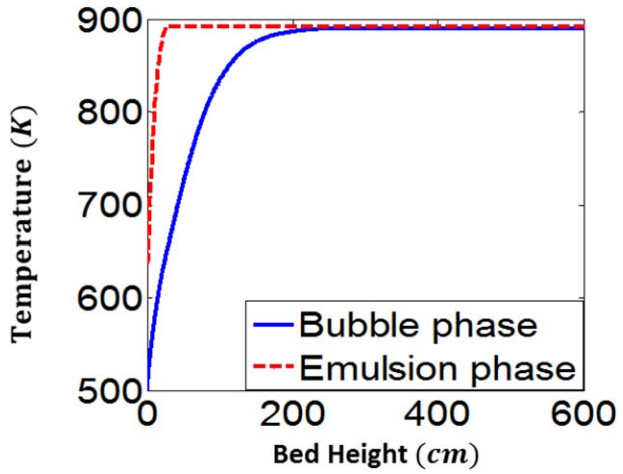

Figure 3. Temperature profile in the emulsion phase and the bubble phase.

[Color figure can be viewed in the online issue, which is available at wileyonlinelibrary.com.]

$$c_{S,e}=c_{S,b}$$

$$c_{H,e}=c_{H,b}$$

$$C_{\mathrm{Si},e}=0$$

We illustrate the behavior of the reaction module by reporting simulation results obtained by solving the differential algebraic equations using the MATLAB solver ODE15s. Simulation results describe the dynamic interplay between emulsion and bubble phases in a bed with height 600 cm. The simulation results in Figure 3 show the temperature profile of the emulsion and bubble phases with respect to the bed height. The bubble phase is heated up due to heat transfer between two phases. The bubble-phase temperature is obtained by solving the energy balances and the emulsion phase temperature is obtained from the fluid dynamics module.

The concentrations of the reactants and product in the bed are calculated together with the temperature profile as illustrated in Figure 3. Figure 4 shows that the concentration dynamics follow temperature change very closely since the reaction rate is a function of temperature. The initial plateau of silane concentration is caused by the low temperature at the entrance of the reactor. Then, a steep decrease occurs in silane concentration near the entry to the bed, at around 7 cm above the inlet gas distributor as illustrated in Figure 4. As the emulsion-phase temperature increases to reaction temperature, silane undergoes an almost complete decomposition and its concentration decreases so that no silane is present at around 25 cm above the distributor. Hydrogen is produced by the silane decomposition and hence its concentration increases very fast along the bed height. It reaches steady state after the silane decomposition is completed as shown in Figure 5. In the part of the bed above the height of 40 cm, the concentrations of silane and hydrogen at emulsion and bubble phases keep unchanged as thermal decomposition of silane takes place immediately once they are fed into the bed from the bottom. Their values are the same as those at the height of 40 cm and therefore they are not shown in Figures 4 and 5 to highlight the changes in the lower part of the bed.

The silicon vapor concentration increases initially because silicon vapor is released from the rapid exothermal reactions just above the distributor as shown in Figure 6. After silicon vapors are generated, they are scavenged by particles for particle growth. As a result, the number of powder particles also decreases after an initial increase which is attributed to homogeneous nucleation and clustering of silicon vapor. The amount of powder particles in the emulsion phase is less than that in the bubble phase because the bubbles contain no seed particle which allows all the silane to react homogeneously, whereas in the emulsion phase, seed particles exist for heterogeneous reaction and hence comparatively less powder as illustrated in Figure 7.

The population balance module

A discrete population balance module describes the dynamics of particle-size distribution in the bed. Particles are distributed among K discrete size intervals. Each interval contains N_i particles each with an average mass m_i. The relationship between the total mass of particles in an interval and the number of particles in the same interval is thereby given by the expression

$$M_i=m_iN_i, \quad \forall i=1,2,...,K. \tag{23}$$

The total surface area of the particles in interval i is given by the expression

$$A_i=a_iN_i$$

where a_i is the surface area of particle i. Experiments show that the silicon particles are nearly spherical so that we have

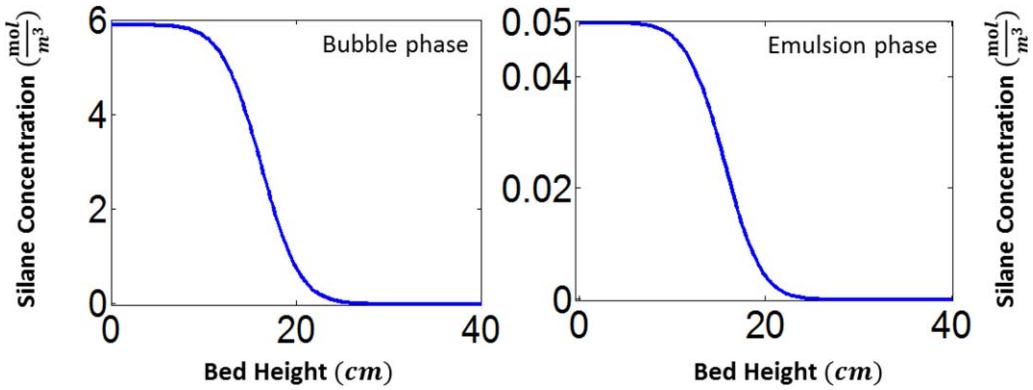

Figure 4. Silane concentration in the emulsion phase and the bubble phase.

[Color figure can be viewed in the online issue, which is available at wileyonlinelibrary.com.]

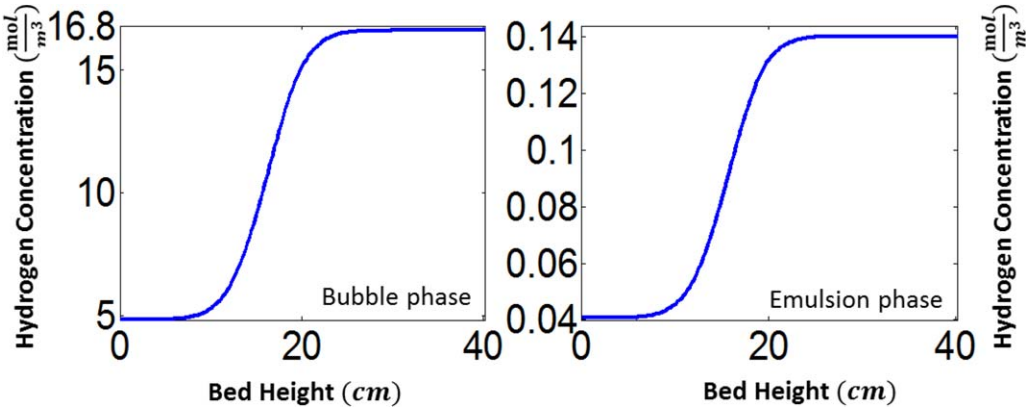

Figure 5. Hydrogen concentration in the emulsion phase and the bubble phase.

[Color figure can be viewed in the online issue, which is available at wileyonlinelibrary.com.]

$$a_i = 4\pi\left(\frac{l}{2}\right)^2$$

where l is the particle diameter. The mass balance for size interval i is written

$$\frac{dM_i}{dt} = q_i + r_i + f_{i-1} - f_i \tag{24}$$

The number balance for this interval is in the form of

$$\frac{dN_i}{dt} = \frac{q_i}{m_i} + \frac{f_{i-1}}{m_i} - \frac{f_i}{m_{i+1}} \tag{25}$$

The rate of addition of particles to interval i by seeding is given by q_i^{in}, whereas the particle withdrawal rate is given by q_i^{out}. The total external flow of particles is represented by

$$q_i = q_i^{\text{in}} - q_i^{\text{out}}$$

The rate of material transfer from the fluid phase to the particles in interval is then represented by

$$r_i = r_{\text{dep}} \frac{A_i}{\sum_i A_i}, \quad \forall i = 1, 2, ..., K-1 \tag{26}$$

As the particles grow, they transition from one size interval to the next. The rate of transition of particles is represented by f_{i-1} for flow into interval i and f_i for flow out of interval i. By comparing the mass balance in Eq. 24 and number balance in Eq. 25 for each size interval, the link flow between neighboring intervals is obtained by the expression,[15]

$$f_i = r_i \frac{m_{i+1}}{m_{i+1} - m_i}$$

We need to pay extra attention to the last interval K as it does not have particle flow to the next interval. The mass balance and number balance for the interval K are rewritten as

$$\begin{aligned} \frac{dM_K}{dt} &= q_K + r_K + f_{N-1} \\ \frac{dN_K}{dt} &= \frac{q_K}{m_K} + \frac{f_{N-1}}{m_K} \end{aligned} \tag{27}$$

By comparing mass balance and number balance for the largest size interval K, we find that

$$r_K = 0 \tag{28}$$

That implies that no mass transfer from gas phase to the particles in the interval K. Simulation results show that particle dynamics reaches steady state after 150 h Average particle size and total surface area of particles are shown in Figure 8. We conclude that particle size increases, whereas the total surface area available for silicon deposition decreases as time evolves.

The fluid dynamics module

The fluid dynamics module predicts the velocity and the bed density of each phase that is solid volume fraction as a

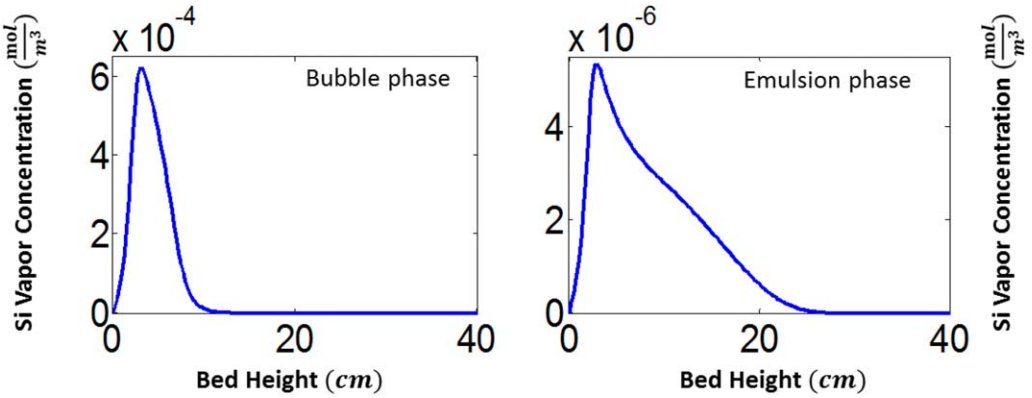

Figure 6. Silicon vapor concentration in the emulsion phase and the bubble phase.

[Color figure can be viewed in the online issue, which is available at wileyonlinelibrary.com.]

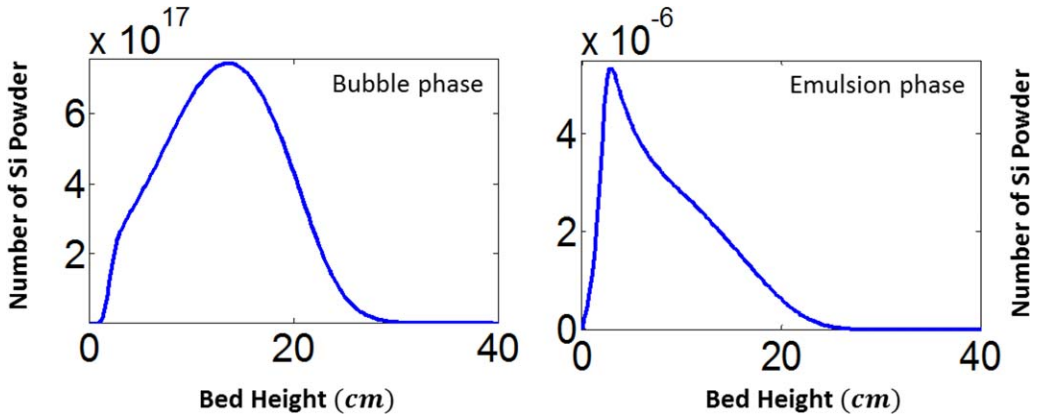

Figure 7. Number of Silicon powder in the emulsion phase and the bubble phase.

[Color figure can be viewed in the online issue, which is available at wileyonlinelibrary.com.]

function of the reactor height. Those obtained profiles are imported into the reaction module consisting of the emulsion and bubble-phase model as illustrated in the previous section. The solid volume fraction also serves as the input to the particle growth module. The average particle size calculated in the particle growth module is sent back to the fluid dynamic module to update parameter information after one simulation cycle.

Solid-phase behavior has a strong influence on the fluid dynamics and plays an important role in shaping the dynamical behavior of the bed. We use a mixture model in which the solids and gas phases are treated as interpenetrating continuums with individual volume fraction. The model tracks the volume fraction and solves for the velocity for each phase. We assume that both phases share the same pressure field. Moreover, the relative velocity between the two phases is essentially determined by pressure, gravity, and viscous drag force. One of the assumptions of a two-phase model is that the emulsion phase operates at minimum fluidization velocity and most of the solids in a fluidized bed are carried in the emulsion phase with only few solids in the bubble phase, which mainly consists of gas with only a wake of solids trailing it. The simulations in the fluid dynamics module were conducted at minimum fluidization velocity which allowed us to make the assumption that we were only simulating the emulsion phase in the fluid dynamics simulation. Therefore, the effect of bubbles on the hydrodynamics is neglected here.

The momentum equation, continuity equation, and transport equation for solid and fluid phases are listed as follows. By solving those equations simultaneously, we obtain the velocity u, the solid volume fraction ϵ_d, and the bed pressure p. The momentum equation is written as

$$\rho\frac{\partial u}{\partial t}+\rho(u\cdot\nabla)u=-\nabla p-\nabla\cdot\left(\frac{\rho\epsilon_d\rho_d}{\rho(1-\epsilon_d\rho_d/\rho)}u_{\text{slip}}u_{\text{slip}}\right)+\nabla\cdot\tau_{gm}+\rho g \tag{29}$$

where τ_{gm} is the sum of viscous and turbulent stresses and is calculated as

$$\tau_{gm}=(\eta+\eta_T)(\nabla u+\nabla u^{\mathrm{T}})-2/3\rho\xi I \tag{30}$$

Continuity equation is in the form of

$$\frac{\partial\rho}{\partial t}+\nabla\cdot\rho u=0 \tag{31}$$

Transport equation for the solid phase is written as

$$\frac{\partial\epsilon_d}{\partial t}+\nabla\cdot(\epsilon_d u-D_{md}\nabla\epsilon_d+\epsilon_d(1-\epsilon_d\rho_d/\rho)u_{\text{slip}})=0 \tag{32}$$

The Hadamard–Rybczynski correlation is used to calculate the drag coefficient between the two phases as

$$C_d=\frac{24}{Re_p}\frac{1+\frac{2}{3}\eta_c/\eta_d}{1+\eta_c/\eta_d} \tag{33}$$

where Re_p is the particle Reynolds number and it is in the form of

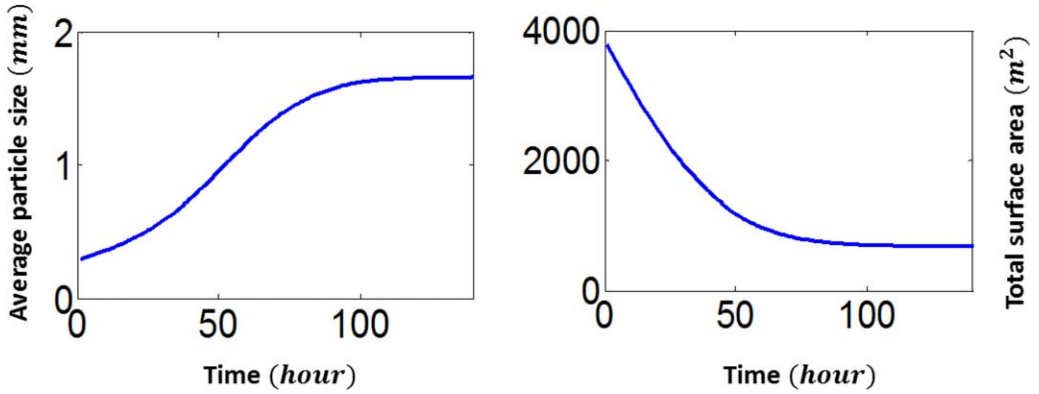

Figure 8. Dynamics of particle growth process.

[Color figure can be viewed in the online issue, which is available at wileyonlinelibrary.com.]

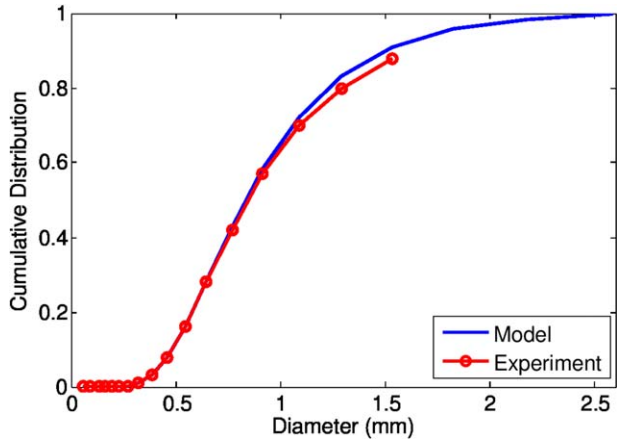

Figure 9. Cumulative mass distribution achieved in a demonstration reactor.

[Color figure can be viewed in the online issue, which is available at wileyonlinelibrary.com.]

$$\mathrm{Re}_p = \frac{d\rho_c |u_{\mathrm{slip}}|}{\eta} \tag{34}$$

d is average particle size. The slip velocity is then calculated as

$$\frac{3}{4}\frac{C_d}{d}\rho |u_{\mathrm{slip}}| u_{\mathrm{slip}} = -\frac{\rho - \rho_d}{\rho}\nabla p \tag{35}$$

Once average particle size is calculated in the particle growth module, they are passed into the fluid dynamics module to update the module parameters. These equations were coded in the COMSOL multiphysics programming environment and solved using the finite element method.

Model Validation and Sensitivity Analysis

In this section, the model is validated against experimental results. A cylindrical bed with height 6 m and diameter 0.3 m was used in the simulation study. The gas mixture containing silane and hydrogen is fed into the bed from the bottom at the volumetric flow rate of $0.03 \mathrm{m}^3/\mathrm{s}$. The mass fraction of silane in the inlet gas is 0.8. The bed pressure is maintained at 1.5 atm. The cumulative mass distribution of silicon particles is obtained using the multiscale model with

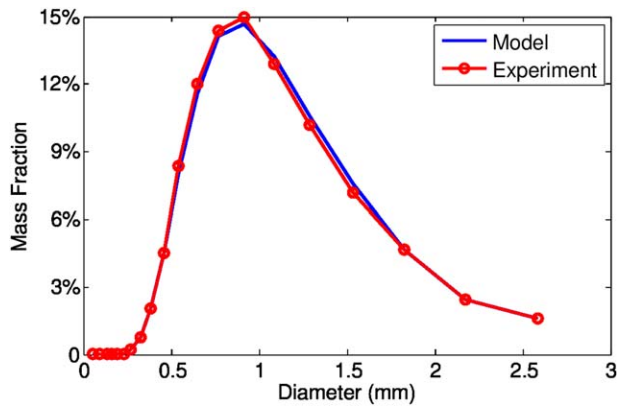

Figure 10. Size distribution achieved a demonstration reactor.

[Color figure can be viewed in the online issue, which is available at wileyonlinelibrary.com.]

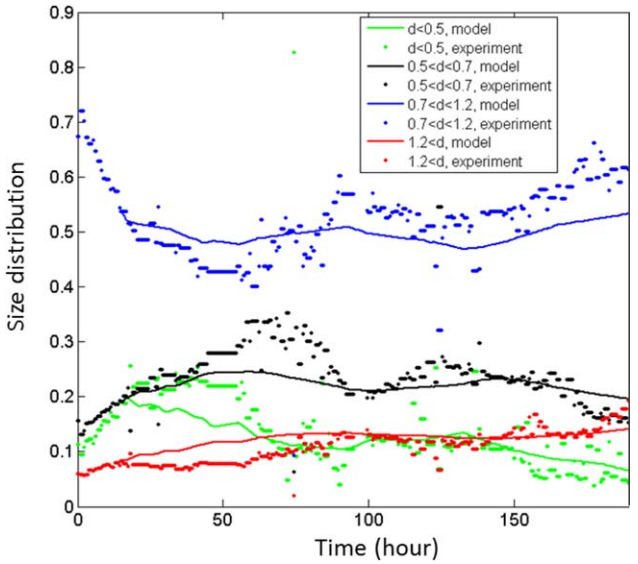

Figure 11. Size distribution achieved in a demonstration reactor.

[Color figure can be viewed in the online issue, which is available at wileyonlinelibrary.com.]

the three modules connected together, as illustrated in Figure 2. Figure 9 shows how the cumulative mass distribution in the simulation compares with the experimental data obtained in a pilot plant. Figure 10 demonstrates that the numerical result of size distribution is in good agreement with experimental results. Those comparisons show that the model enables to predict size distributions of silicon particles produced in the FBR.

The uncertainty of particle growth rate has implications on the design of control strategy. Figure 11 shows that how the size distribution of particles evolves as a function of time. It is clear that while the model tracks the average size, the simulation and the experiment show that the particle-size distribution function evolves slowly. The time for the system to reach steady state is estimated to be 150 h.

To investigate the effect of process parameters and operating conditions on the process dynamics, we perform sensitivity studies on the multiscale model. The mass fraction of silane in the inlet gas directly affect the further thermal decomposition and hence the resulting particle-size distribution. The other important parameter is the flow rate of inlet gas. The fluidization dynamics highly depends on the inlet gas velocity. Transport phenomena between the emulsion phase and the bubble phase is affected by fluidization condition which has an indirect influence on particle behavior as a consequence.

Inlet flow rate

We adjust the inlet flow rate of mixed gas in the range of 0.02–0.05 m^3/s while all the parameters are kept constant. We expect to see that similar effect on the average diameter and deposition rate as increasing mass fraction of silane in the feeding gas in Figure 12. Higher flow rate provides more silane for decomposition. That directly causes the increase of silicon deposition rate which leads to the increase of average size of particle product. A decrease in powder formation is observed as we go from low to high flow rates. One of the primary operational parameters is to quantify the amount of silicon lost as powder. A lower total surface area is obtained

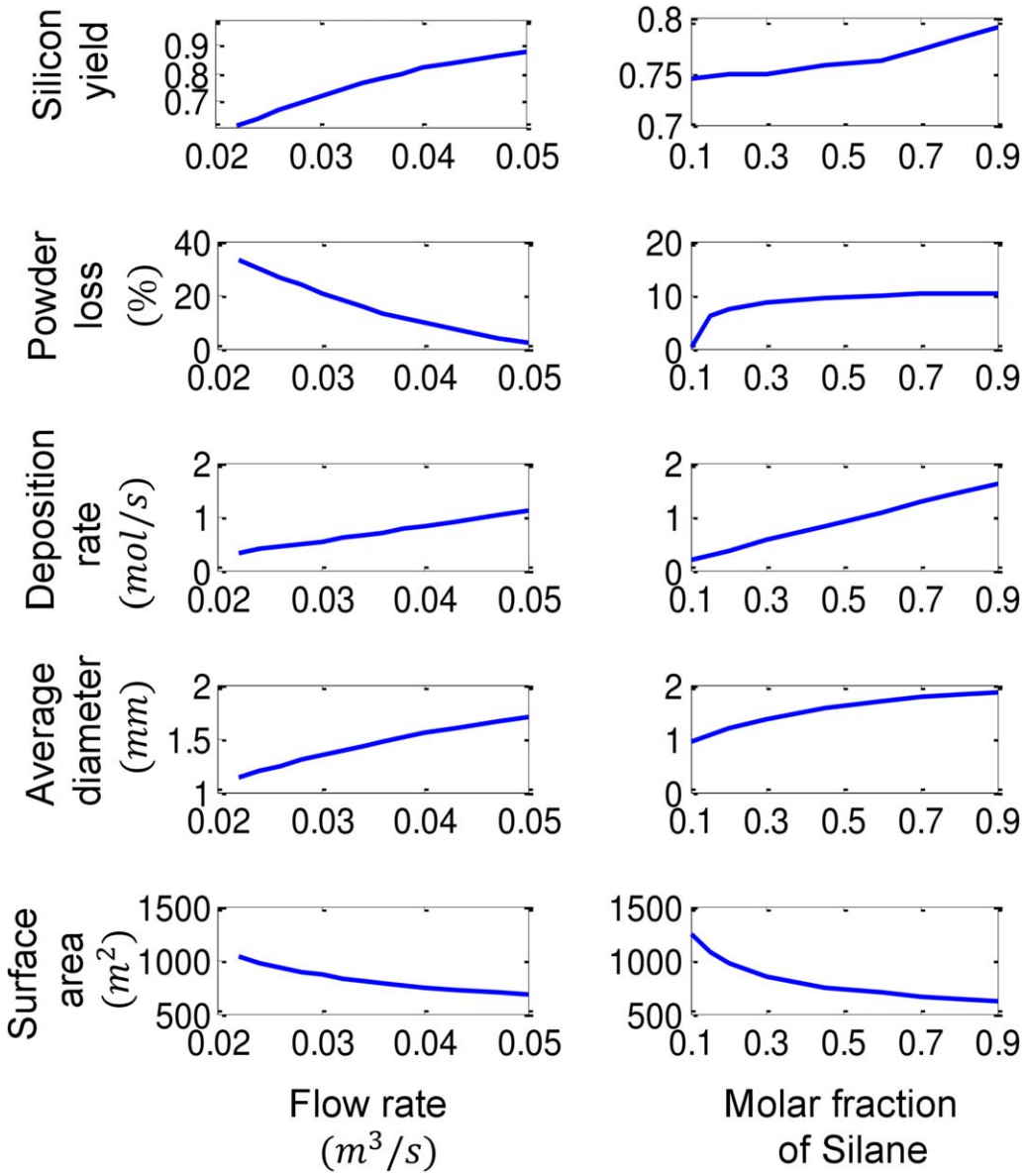

Figure 12. Sensitivity analysis.

[Color figure can be viewed in the online issue, which is available at wileyonlinelibrary.com.]

due to the increase of deposition rate. We also observe the decline of the amount of powder. With higher flow rate, more powder is entrained in the gas and exit from the top and thus the loss of powder is increased. We conclude that the yield of silicon increases as the inlet flow rate is higher within the range discussed here.

Mass fraction of silane

The mass fraction of silane in the feed mixture of silane and hydrogen is varied in the range of 0.1–0.9. Figure 12 shows that as more silane molecules are available to decompose, the yield of silicon increases. The average size of particles increases as a result of increase in the mass fraction of silane with respect to hydrogen in the feed gas. This is due to the increase of silicon vapors released from thermal decomposition of silane which leads to larger deposition and scavenging rate. In addition to the increasing deposition rate, a rise in the amount of powder generated is also observed with the rise in inlet silane concentration. This is because although total deposition rate increases, more silane molecules are present in the reactor causing them to undergo homogeneous reaction and subsequent nucleation to form powder. The surface areas reduce as mixed gas with higher silane concentration is fed. This is due to the increase of silicon deposition rate as explained previously for the decrease of total surface areas when they reach steady state. We draw the conclusion that mole available silane molecules gives higher silicon yield.

Passivity-Based Inventory Control Strategy

In this section, we develop passivity-based inventory control strategy for total mass, energy, and average particle size in the FBR. We review passivity-based inventory control first and design an inventory control system for this specific particulate process.

Conservation laws in terms of inventories such as mass and internal energy are in the general form of

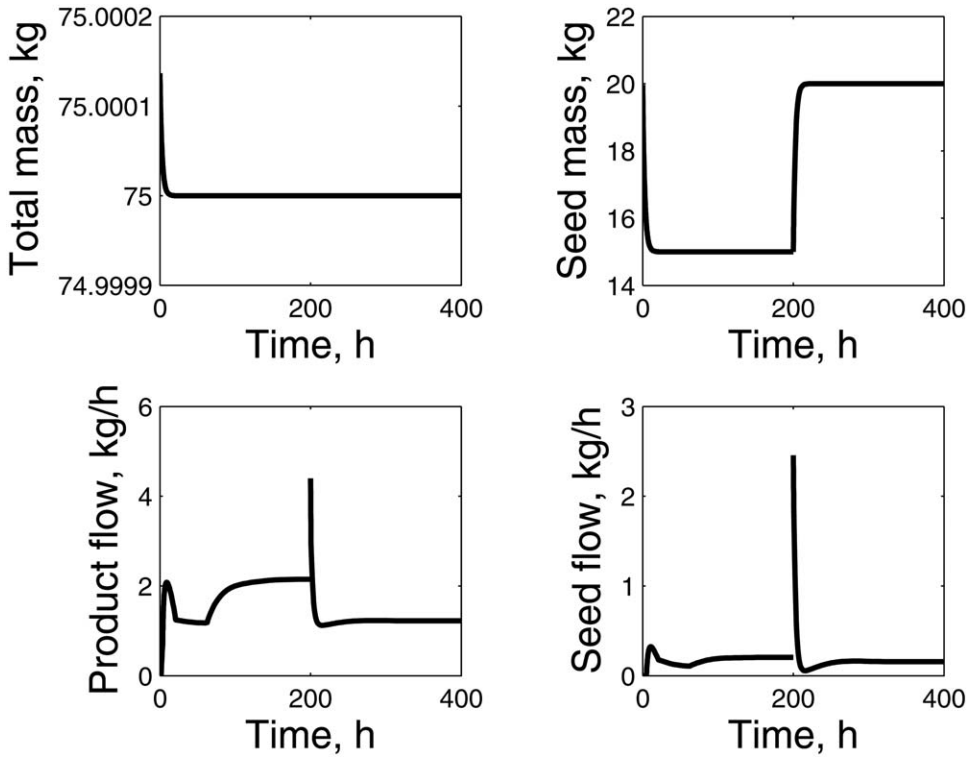

Figure 13. Control total and seed hold up.

$$\frac{dZ}{dt}=p(Z,m)+\phi(Z)m \tag{36}$$

where Z is the inventory, m is the vector of manipulated variables, $p(\cdot)$ is the production rate, and $\phi(\cdot)$ is the supply rate. Furthermore, $\phi(Z)$ needs to be nonzero to ensure controllability. The feedback–feedforward control law is in the following form to make the controlled inventory Z_c follow their set points Z_c^*

$$m=\phi(Z)^{-1}\left(-\mathbf{C}(Z-Z^*)-p(Z,m)+\frac{dZ^*}{dt}\right) \tag{37}$$

where $\mathbf{C}$ is a strictly input passive operator. The feedback–feedforward control law gives us input–output stability, so called passivity, of the closed loop system. We review briefly how to achieve the passivity of the closed loop system using inventory control as below. Let $p(Z,m)+\phi(Z)m$ be the synthetic input u and $Z-Z^*$ be the synthetic output y, then we have

$$\mathrm{u}^{\mathrm{T}}\mathrm{y}=\left(-\mathbf{C}(Z-Z^*)+\frac{dZ^*}{dt}\right)^{\mathrm{T}}(Z-Z^*) \tag{38}$$

Substituting the control law into the open loop dynamics in Eq. 36, we obtain the dynamics of the closed loop system

$$\frac{d(Z-Z^*)}{dt}=-\mathbf{C}(Z-Z^*) \tag{39}$$

Thus, we have

$$\mathrm{u}^{\mathrm{T}}\mathrm{y}=\frac{d(Z-Z^*)^{\mathrm{T}}}{dt}(Z-Z^*) \tag{40}$$

We choose the storage function of the closed loop system as $W=1/2(Z-Z^*)^{\mathrm{T}}(Z-Z^*)$, then we enforce the closed loop system to be passive as follows

$$\mathrm{u}^{\mathrm{T}}\mathrm{y}=\frac{dW}{dt} \tag{41}$$

Many examples of control strategies are strictly input passive. The Proportional-Integral Derivative Control (PID) control, for example

$$\mathbf{C}(e)=K_c\left(e+\frac{1}{\tau_I}\int_0^t e(\tau)d\tau+\tau_D\frac{de}{dt}\right) \tag{42}$$

where $e=Z_c-Z_c^*$. It is strictly input passive for any $K_c,\tau_I,\tau_D>0$. The rate of exponential decay of the error e is determined by the controller gain.

We develop a three layer inventory control system: the first tier provides control of the total mass balance; the second tier controls the energy balance control which is built on total mass control; the third tier provides seed balance control and it regulates the process so that we obtain a desired average particle size.

Mass balance control

In this simulation study, we use the validated multiscale model to calculate silicon yield and then implemented control strategy on the multiscale model. Total mass of particles needs to be controlled to maintain the bed at a constant level. A constant bed level implies that the bed has a constant pressure drop which signals stable fluidization. The mass balance for total hold up of silicon is written as

$$\frac{dM}{dt}=S+Y-W \tag{43}$$

where S is seed flow rate, Y is silicon production yield, and W is product withdrawal rate. We select W as manipulated variable to control total mass of silicon M. A proportional control law is used here to illustrate how to design an

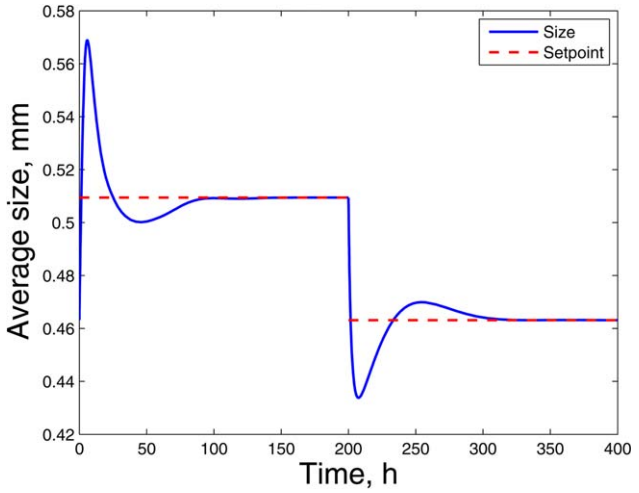

Figure 14. Particle size achieved during seed control of PBM.

[Color figure can be viewed in the online issue, which is available at wileyonlinelibrary.com.]

inventory controller. The proportional control gain is selected as $K_m=0.01$. We then have

$$\frac{d(M-M^*)}{dt}=-K_m(M-M^*) \tag{44}$$

Substituting the mass balance equation into the foregoing control law, we obtain the explicit expression for manipulated variable W

$$W=S+Y+K_m(M-M^*) \tag{45}$$

Thus, the mass balance controller uses a combined feedforward and feedback law to maintain the total silicon mass at a desired value.

Seed balance control

The particle-size distribution in the FBR can be altered by manipulating the ratio of seed mass to total mass as shown by Du and Ydstie.[19] Therefore, to achieve desired average particle size, we change the ratio of seed to total mass of particles. The size interval mass balance is written as

$$\frac{dM_i}{dt}=y_i+s_i-w_i \tag{46}$$

where y_i represents production and internal flow terms between size intervals, s_i and w_i represent seed addition rate and product withdrawal rate at each size interval i. Compare with the mass balance in Eq. 43, we have the constitutive relation

$$Y=\sum_{i=1}^{K} y_i$$

$$S=\sum_{i=1}^{K} s_i$$

$$W=\sum_{i=1}^{K} w_i$$

The mass of seed particles follows its setpoint M^*_{seed} by manipulating seed addition rate S based on the following control law

$$S=-\sum_{i=1}^{I_s} y_i-\sum_{i=1}^{I_s} w_i-K_s\left(\sum_{i=1}^{I_s} M_i-M^*_{\text{seed}}\right) \tag{47}$$

where the controller gain is chosen as $K_s=0.0001$. The total mass of seed particles are the summation of particle mass from size interval 1 to interval I_s. g_i is the silicon production rate in each size interval. In this simulation, we assumed that the largest seed size interval, I_s, was interval 10 out of 20 and that the distribution of seed particles flowing into the system was constant. The needed seeds are generated by an external reactor, which aims at producing small seed particles for this FBR. The seed-size distribution is predetermined and thus I_s in Eq. 47 is prior.

Simulation of controlling the total and seed particle hold up is shown in Figure 13. The hold up of particles in the system is shown in Figure 13. The product and seed flow rates required to achieve the control are also shown.

The average particle-size and size distribution achieved during each steady state are shown in Figure 14. This simulation shows we can control the average product size as well as the product distribution. As the hold up of seed particles increases relative to the total hold up, the average size decreases. The interval representation of the size distribution supports this result.

Conclusions

We developed and tested a model and control scheme for a FBR for the production of solar-grade silicon. A population balance describes particle-size distribution is integrated with a fluid dynamics model which represents the hydrodynamics of the fluidized bed reactor. The proposed steady-state analysis demonstrates the cumulative fraction of particles with respective to particle size. Finally a multivariable inventory controller is developed for the FBR. Simulation results demonstrate that the inventory controller can be used to control the size distribution of particles. The proposed modeling and control approach provides an effective way to investigate reactor performance and final product property.

Notation

z = height from bottom of fluidized bed, cm
u_{Gb} = superficial bubble velocity in emulsion phase, cm/s
u_{Ge} = superficial gas velocity, cm/s
u_b = superficial bubble velocity, cm/s
ϵ_{mf} = void fraction at minimum fluidizing conditions
ϵ_b = void fraction in packed bed
ϵ_f = void fraction in bubbling bed
a = ratio of wake volume to bubble volume
$c_{S,b}$ = concentration of SiH_4 in the gas bubbles, mol/cm^3
$c_{S,j}$ = concentration of SiH_4 in the grid region, mol/cm^3
δ_b = void fraction of bubbles in the bed
β_b = coagulation coefficient, cm^3/s
K_{be} = bubble-emulsion mass-transfer coefficient, cm/s
$c_{S,e}$ = concentration of SiH_4 in the back-mixed reactor, mol/cm^3
r_{HD} = rate of homogeneous decomposition of SiH_4, mol/cm^3s
r_{HT} = rate of heterogenous chemical vapor deposition of SiH_4, mol/cm^2s
ϕ_S = sphericity of a particle
$M_{2/3}$ = moments of size distribution density funciton
r_{DF} = Rate of molecular bombardment of Si vapor on powder, mol/cm^2s
r_{HN} = rate of homogeneous nucleation, mol/cm^3s
$\bar{c}_p$ = specific heat of gas phase, J/g K
T_b = temperature in the gas bubbles, K
T_e = temperature in the emulsion bubbles, K
$(H_{be})_b$ = volumetric heat-transfer coefficient, J/cm^3sK
A_{TL} = total surface area of seed particles, m^2
V_I = total volume of gas phase, m^3

μ = gas viscosity, kg/(sm)
M_0 = total number of particles per unit volume gas, cm^{-3}
M_1 = total volume of particles per unit volume gas, cm^3/cm^3
v_b = bubble volume, cm^3
v^* = critical volume of powder produced by homogeneous nucleation, cm^3
α = specific surface of solid per volume of bed, cm^{-1}
c_{Si} = concentration of Si vapor, mol/cm^3
c^*_{Si} = the supersaturated concentration of Si vapor, mol/cm^3
d_p = average particle diameter, m
D = particle diffusion coefficient, cm^2/s
D_g = gas diffusion coefficient, cm^2/s
μ = velocity, m/s
u_{slip} = the relative velocity between two phases, m/s
ρ = the bed density, kg/m^3
ρ_c = density of the gas mixture, kg/m^3
p = the bed pressure, Pa
ϵ_d = solid volume fraction
η_d = the solid viscosity, Pa s
η_T = turbulent viscosity, Pa s
D_{md} = turbulent dispersion coefficient, m^2/s
k = thermal conductivity, W/m/K
k_T = turbulent thermal conductivity, W/m/K
m_{dc} = mass transfer from solid phase to gas phase, $kg/m^2/s$
p = pressure, Pa
Re_p = particle Reynolds number
c_p = the specific heat capacity, J/K/mol
α_c = condensation coefficient, 0.05
N_A = Avogadro's number, 6.023×10^{23}
R = gas constant, 1.986cal/K/mol
m = molecular mass of SiH_4, 32 g/mol
k_B = Boltzmann's constant, 1.38×10^{-23}J/K
d_{pf} = average powder diameter, 0.3×10^{-6}m
g = acceleration of gravity, $980cm/s^2$
T_1 = reference temperature, 1412 K
$\bar{\sigma}_1$ = reference specific surface free energy, $0.736J/cm^2$
ρ = silicon density, $2300kg/m^3$
M_{Si} = molar mass of Si, 28 g/mol
μ = viscosity, $1.75\times10^{-4}kg/s/m$
q_f = inlet gas flow rate, 0.025 mol/s
c_{Sf} = concentration of SiH_4 in the feed gas, $6mol/m^3$
c_{Hf} = concentration of H_2 in the feed gas, $24mol/m^3$
A_t = cross-sectional area of the bed, 0.07 m^2
T_f = feed temperature, 500 K
K = total number of size intervals, 20
ρ_d = density of solid phase, $2300kg/m^3$
g = gravitational acceleration, $9.81m/s^2$

Literature Cited

1. Masson G, Latour M, Rekinger M, Theologitis T, Papoutsi M. *Global Market Outlook For Photovoltaics*. European Photovoltaic Industry Association, Belgium, 2013.
2. Ranjan S, Balaji S, Panella RA, Ydstie BE. Silicon solar cell production. *Comput Chem Eng*. 2011;35(8):1439–1453.
3. Lutwack G. *Flat-Plate Solar Array Project Final Report*: Vol II, DOE/JPL-1012–125, USA, 1986.
4. Lai S, Dudukovic M, Ramachandran P. Chemical vapor deposition and homogeneous nucleation in fluidized bed reactors: silicon from silane. *Chem Eng Sci*. 1986;41:633–641.
5. Kunii D, Levenspiel O. *Fluidization Engineering*. Butterworh-Heinamann, Oxford, UK, 1991.
6. Davidson J, Harrison D. *Fluidized Particles*. New York: Cambridge University Press, 1963.
7. Caussat B, Hemati M, Couderc J. Silicon deposition from silane or disilane in a fluidized bed. *Chem Eng Sci*. 1995;50(22): 3615–3624.
8. Lai S. *Modeling of Fluidized Bed Reactors for Manufacture of Silicon from Silane*, Saint Louis, MO: Washington University, 1987.
9. Pina J, Bucala V, Schbib NS, Ege P, de Lasa HI. Modeling a silicon CVD spouted bed pilot plant reactor. *Int J Chem React Eng*. 2006; 4(1).
10. Huang Y, Ramachandran PA, Dudukovic MP. *Fluidized Bubbling Bed Reactor Model for Silane Pyrolysis in Solar Grade Silicon Production*. AIChE Annual Meeting, Salt Lake City, UT, 2007.
11. Guenther C, O'Brien T, Syamlal M. A Numerical Model of Silane Pyrolysis in a Gas-Solids Fluidized Bed. In: *Proceedings of the International Conference on Multiphase Flows*. New Orleans, 2001.
12. Cadoret L, Reuge N, Pannala S, Syamlal M, Caussat B. Silicon CVD on powders in fluidized bed: experimental and multifluid Eulerian modelling study. *Surf Coat Technol*. 2007; 201(22):8919–8923.
13. Cadoret L, Reuge N, Pannala S, Syamlal M, Rossignol C, Dexpert-Ghys J, Coufort C, Caussat B. Silicon Chemical Vapor Deposition on macro and submicron powders in a fluidized bed. *Powder Technol*. 2009;190(1):185–191.
14. Hsu G, Levin H, Hogle R, Praturi A, Lutwack R. Fluidized bed silicon deposition from silane. *US Patent* 4,314,525, 1982.
15. White C, Ege P, Ydstie BE. Size distribution modeling for fluidized bed solar grade silicon production. *Powder Technol*. 2006;163: 51–58.
16. Sukumar B, Du J, White CM, Ydstie BE. Multiscale modeling and control of fluidized beds for the production of solar grades Silicon. *Powder Technol*. 2009;1:23–31.
17. Yaws CL. *Transport Properties of Chemicals and Hydrocarbons*. Norwich, NY: William Andrew, 2009.
18. Yaws CL. *The Yaws' Handbook of Physical Properties for Hydrocarbons and Chemicals*, Gulf Pub. Co. 2005.
19. Du J, Ydstie BE. Modeling and control of particulate processes and application to poly-silicon production. *Chem Eng Sci*. 2012;67(1): 120–130.
20. Hogness TR, Wilson TL, Johnson WC. The thermal decomposition of silane. *J Am Chem Soc*. 1936;58(1):108–112.
21. Abraham FF. *Homogeneous Nucleation Theory*. New York: Academic Press, 1974.
22. Friedlander SK. *Smoke, Dust and Haze: Fundamentals of Aerosol Behavior*. New York: Wiley-Interscience, 1977.
23. Iya SK, Flagella RN, DiPaolo FS. Heterogeneous decomposition of silane in a fixed bed reactor. *J Electrochem Soc*. 1982;129(7): 1531–1535.
24. Dutta S. *Multiscale Modeling of Fluidized Bed Reactor for Production of Polysilicon*. Pittsburgh, PA: Carnegie Mellon University, 2012.

Manuscript received Sept. 5, 2013, and revision received Dec. 16, 2013.